High-Temperature Mechanical Behavior of Cold-Worked Stress-Relieved Zr-2.5Nb

K. Kapoor, K. Murlidharan, and K.M. Sreedharan

The mechanical behavior of cold-worked stress-relieved Zr-2.5Nb pressure tube material used in pressurized heavy-water reactors is summarized in terms of ultimate tensile strength (UTS), yield strength (YS), and percentage elongation to fracture, strain-rate sensitivity (m), strain-hardening index (n), and activation energy for the self-diffusion of zirconium. Tensile tests carried out in the temperature range of 298 to 773 K at three different strain rates are used to calculate n and m. At higher temperatures, UTS, YS, percentage elongation, and n are found to be strain rate dependent. The plateaus observed in curves for UTS or YS versus temperature are typical of dynamic strain aging behavior. The drop in strength at high temperature is correlated with the self-diffusion of zirconium in α-phase zirconium by comparing the activation energies of the two phenomena. Transmission electron microstructures of thin foils from samples tested at ambient temperature and at 773 K are used to explain the observed variation of n and m with test temperature. A similar trend in the variation of m and percentage elongation with temperature is also explained.

Keywords

activation energy, dynamic strain aging, percentage elongation, self-diffusion, strain hardening index, strain rate sensitivity, ultimate tensile strength, yield strength, Zr-2.5Nb,

1. Introduction

ZIRCONIUM containing 2.5 wt% Nb is often used as a structural material for pressure tubes in pressurized heavy-water reactors at operating temperatures of 523 to 588 K. Tensile tests are routinely carried out at 573 K to evaluate mechanical properties of these tubes in the as-fabricated condition. Tensile tests reported here cover a wide range (i.e., operation temperature ± 200 K).

Such tubes undergo significant changes in strength and microstructure during service in reactors due to irradiation creep and growth (Ref 1). Tests conducted in this study in the temperature range of 573 to 773 K represent accelerated tests for changes taking place after an extended period at reactor operating temperature. However, changes occurring due to irradiation were not considered. A limited amount of data on high-temperature mechanical behavior is available in this respect, mostly dealing with either heat-treated alloy (Ref 2, 3) or tubes produced by a different method, such as drawing the extruded blank with total cold work of 22 to 25% (Ref 4). Efforts have been made in this study to analyze the high-temperature tensile data obtained in terms of strain-rate sensitivity, strain-hardening index, activation energy, and so on.

Fabrication of the Zr-2.5Nb pressure tube used in this study involves extrusion of preheated β-quenched billets, which have a fine martensitic structure (Fig. 1a), to hollow blanks. These blanks are pilgered in two stages to final size, with an intermediate annealing at 823 K for 6 h in vacuum. The tubes are then stress relieved in an autoclave. This process develops a very fine two-phase structure of strongly textured, elongated α grains and a grain-boundary network of β-Zr phase (Fig. 1b).

K. Kapoor and **K.M. Sreedharan,** Nuclear Fuel Complex, Hyderabad, India; **K. Murlidharan,** Defence Metallurgical Research Laboratory, Hyderabad, India

2. Experimental Technique

Tubes of Zr-2.5Nb were analyzed for chemical composition (Table 1). Specimens for tensile testing were machined from longitudinal sections of the tubes. Tests were conducted on a universal testing machine supplied by M/s. Instron, Canton, MA (model-1185). High-temperature tests were conducted in air using a split-type tubular resistance furnace. Extensometers were connected to the grips in order to plot load versus stroke data on a strip chart recorder. The temperature of the specimens during soaking and testing was controlled to within ± 0.2 K, and a temperature variation of less than 2 K was maintained along the gage length. Tests were conducted at strain rates of 4.44×10^{-3}/s, 4.44×10^{-4}/s, and 4.44×10^{-5}/s at room temperature and at 50 K intervals in the range of 423 to 773 K. The specimens were soaked for 45 min at the test temperature in order to attain thermal equilibrium. Immediately after fracture, the specimens were air cooled by removing the surrounding furnace. Load/stroke data were converted to true stress/true strain data using standard equations with a computerized routine.

Table 1 Typical chemical analysis of Zr-2.5Nb pressure tube material

Element	Composition	
	Specified	By analysis
Niobium, %	2.3-2.8	2.60
Oxygen, ppm	900-1300	1150
Iron, ppm	1500 max	1210
Chromium, ppm	200 max	150
Tin, ppm	100 max	<25
Copper, ppm	30 max	<30
Nitrogen, ppm	65 max	39
Hydrogen, ppm	25 max	<10
Zirconium	...	bal

Gage portions of fractured specimens corresponding to each test temperature extremum were examined microscopically. Thin foils were prepared by a twin-jet electroetching technique using a solution of methanol containing 10% lactic acid, 7% sulfuric acid, 3% nitric acid, and 2% hydrofluoric acid at 243 K. These foils were examined under a transmission electron microscope (TEM).

3. Results

3.1 *Mechanical Properties*

Tensile data were obtained in the form of load versus extension. These data were used to determine 0.2% yield stress (YS), ultimate tensile strength (UTS), and ductility (percentage elon-

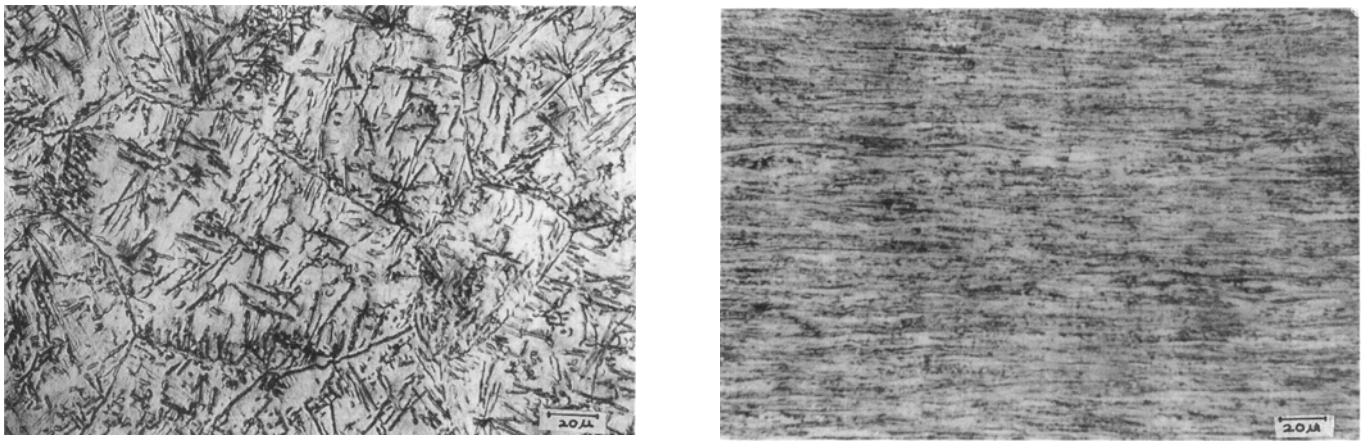

(a) (b)

Fig. 1 Optical micrographs under polarized light. (a) Billet microstructure showing fine acicular martensite. (b) As-fabricated tube microstructure showing a fine fibrous α + β-phase structure

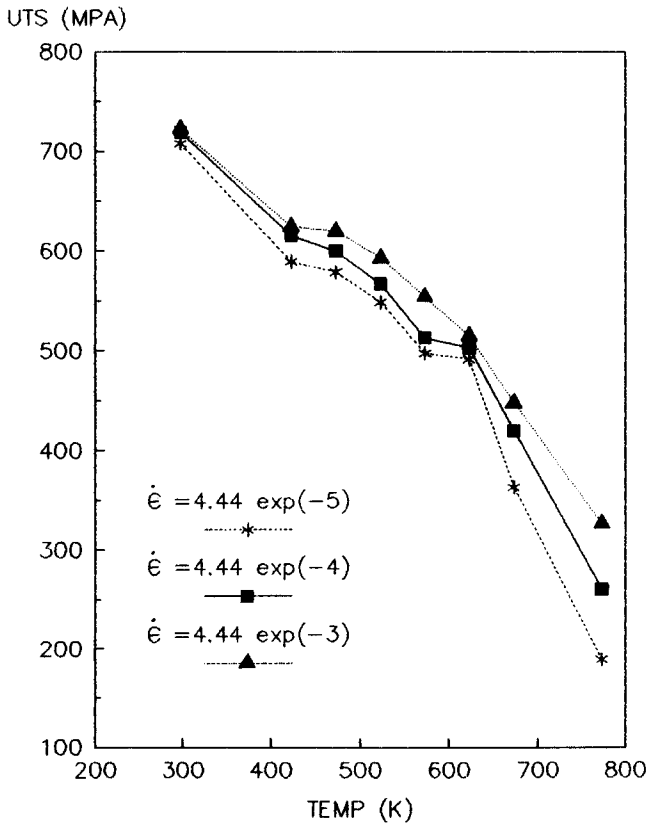

Fig. 2 Ultimate tensile strength as a function of test temperature

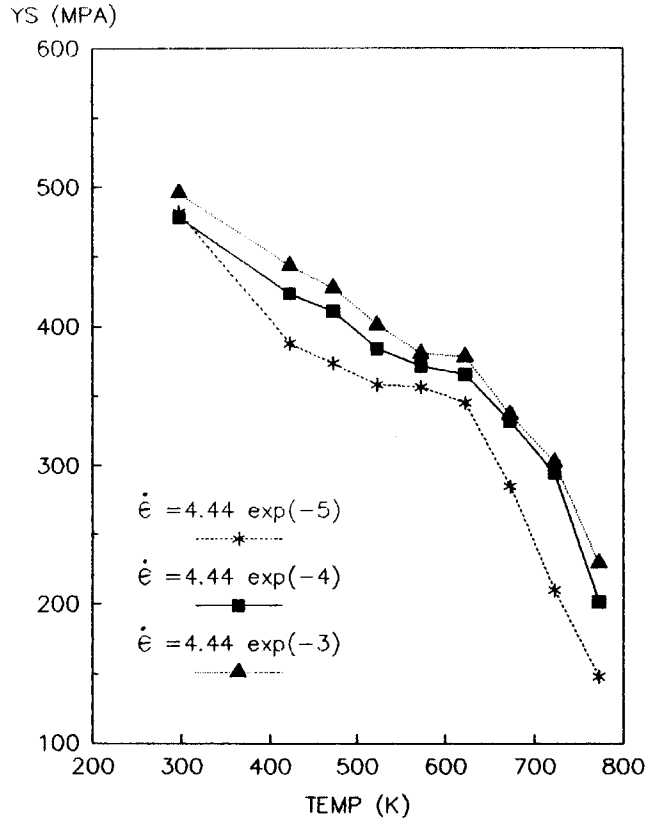

Fig. 3 0.2% yield strength as a function of test temperature

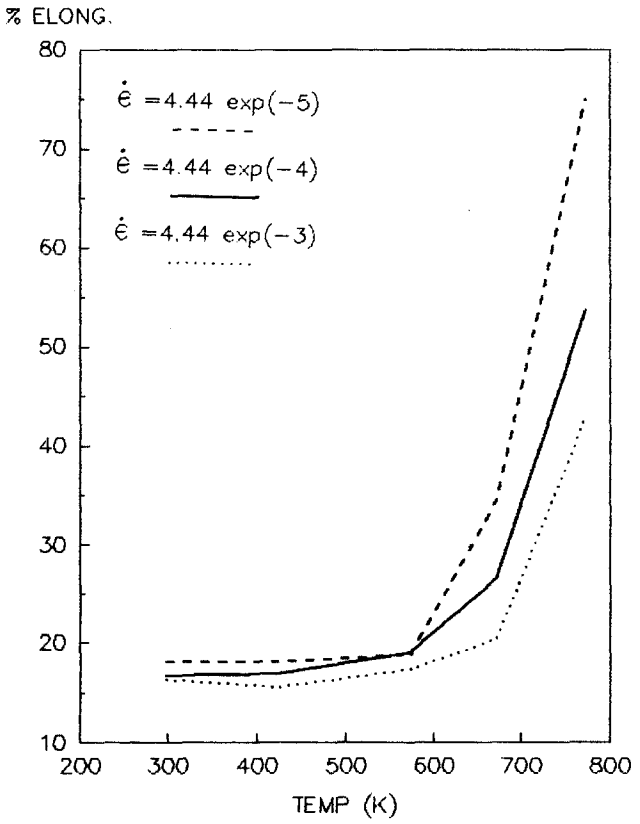

Fig. 4 Percentage elongation as a function of test temperature

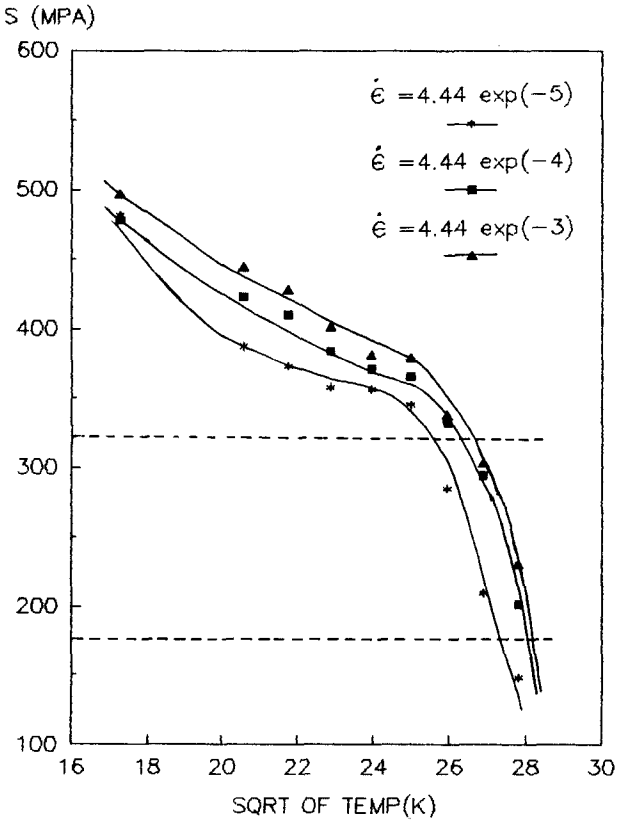

Fig. 5 0.2% yield strength as a function of the square root of absolute test temperature

gation) at various temperatures and strain rates. Plots representing variations of UTS, 0.2% YS, and percentage elongation with test temperature for various strain rates are presented in Fig. 2 to 4, respectively. These results indicate that at constant strain rate, 0.2% YS and UTS decrease slowly from room temperature to about 450 K. they remain nearly constant, in the form of a plateau, from 450 to 625 K and then decrease rapidly at temperatures greater than 625 K. The strain-rate effect can also be observed from these plots. At a given temperature, a slower strain rate lowers the strength value.

An empirical relationship between yield stress and the square root of the test temperature at constant strain rate (Ref 5) is given by:

$$\sigma_T = \sigma_0 - sT^{1/2} \qquad \text{(Eq 1)}$$

where σ_T is the yield strength at test temperature T, σ_0 is the yield strength at absolute zero, and s is the slope of the line. Plots obtained from Eq 1 for three different strain rates are shown in Fig. 5. For a given strain rate, the value of s varies with temperature. In order to study the kinetics of the process responsible for loss of yield strength at elevated temperatures, tie lines at YS = 175 MPa and YS = 315 MPa were drawn parallel to the x-axis intersecting the three strain-rate plots and the corresponding temperature values noted. These strain rates were plotted on a logarithmic scale against the reciprocals of the temperature values obtained (Fig. 6 and 7). According to the Arrhenius equation:

$$\dot{\varepsilon} = A\exp\left(\frac{-Q}{RT}\right) \qquad \text{(A)}$$

or

$$\ln(\dot{\varepsilon}) = \ln A + \left(\frac{-Q}{R}\right)\left(\frac{1}{T}\right) \qquad \text{(B)}$$

where $\dot{\varepsilon}$ is strain rate, Q is activation energy, R is the universal gas constant, and A is a constant. The slope of a plot of ln ($\dot{\varepsilon}$) versus ($1/T$) is equal to ($-Q/R$). This gives an activation energy, Q, equal to 86.6 kJ/mol for YS = 175 MPa (Fig. 6) and 99.8 kJ/mol for YS = 315 MPa (Fig. 7).

The load versus extension data were converted to true stress/true strain data by standard plastic stress-strain equations and are shown in Fig. 8 and 9. The following observations can be made from these plots:

- At constant temperature, the flow stress increases with increasing strain rate.
- At constant strain, the flow stress decreases with increasing temperature.

The original Ludwigson equation (Ref 6) gives the flow stress (σ) at constant strain rate ($\dot{\varepsilon}$) and temperature (T) as:

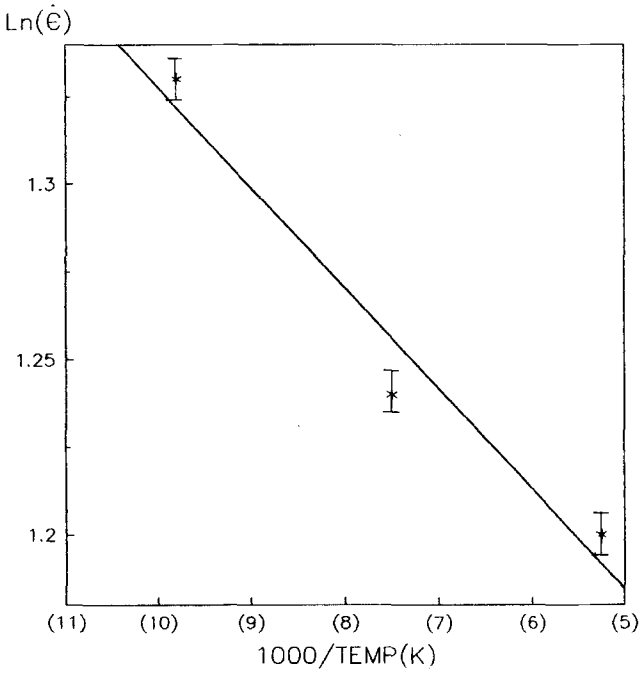

Fig. 6 Arrhenius plot of ln ($\dot{\varepsilon}$) as a function of the reciprocal of test temperature corresponding to a constant yield strength of 175 MPa

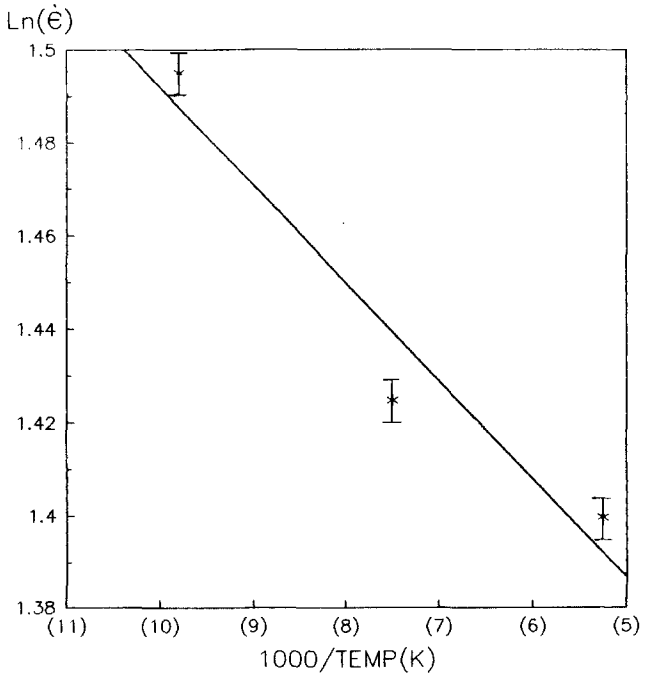

Fig. 7 Arrhenius plot of ln ($\dot{\varepsilon}$) as a function of the reciprocal of test temperature corresponding a constant yield strength of 315 MPa

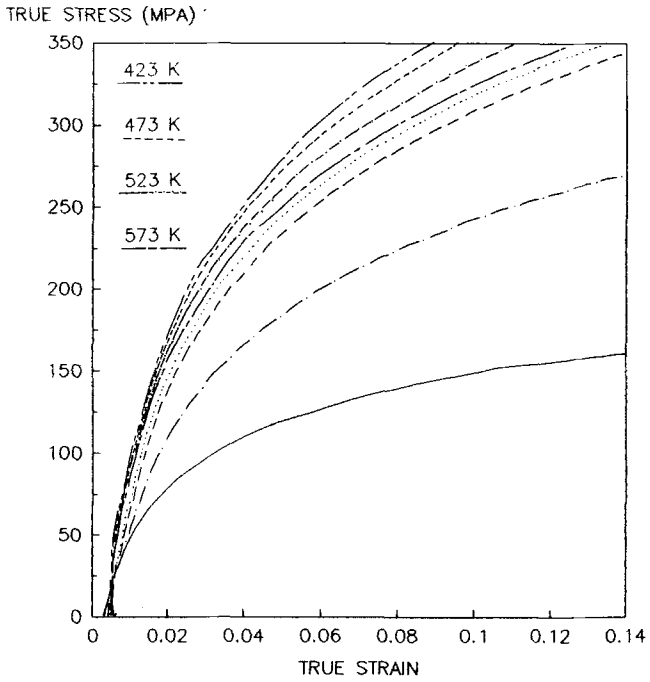

Fig. 8 True stress/true strain curve (numerical fit of the data) at a constant strain rate of 4.44×10^{-4}/s and different temperatures

$$\sigma = A\varepsilon^n + \exp(B + n\varepsilon) \quad \text{(Eq 2)}$$

where ε is true strain, n is the strain-hardening index, and A and B are material constants. An equation representing plastic deformation at low temperature and low strain values can be obtained from Eq 2:

$$\sigma = K_1 \varepsilon^n|_{T,\dot{\varepsilon}} \quad \text{(Eq 3)}$$

where K_1 is a constant.

To calculate the strain-hardening index, n, the log of true plastic stress was plotted against the log of true plastic strain; n was calculated from the slope of these curves (Fig. 10). For all test temperatures and strain rates, n can be calculated in a similar way. These values of n are drawn in the form of a curve in Fig. 11. The following observations can be made:

- The strain-hardening index drops with an increase in temperature.
- At a given temperature, the higher the strain rate, the higher the strain-hardening index (n). This is more prominent at higher temperatures; that is, at lower temperatures the strain-rate effect on n is less.

However, at elevated temperatures with fixed strain and temperature, the flow stress is strain rate dependent and is given by Eq 4 (Ref 7):

$$\sigma = K_2 \dot{\varepsilon}^m|_{T,\varepsilon} \quad \text{(Eq 4)}$$

where $\dot{\varepsilon}$ is strain rate, m is strain-rate sensitivity, and K_2 is a material constant. Values of m can be evaluated from the slope of log (0.2% YS) versus log ($\dot{\varepsilon}$) plots for various temperatures as

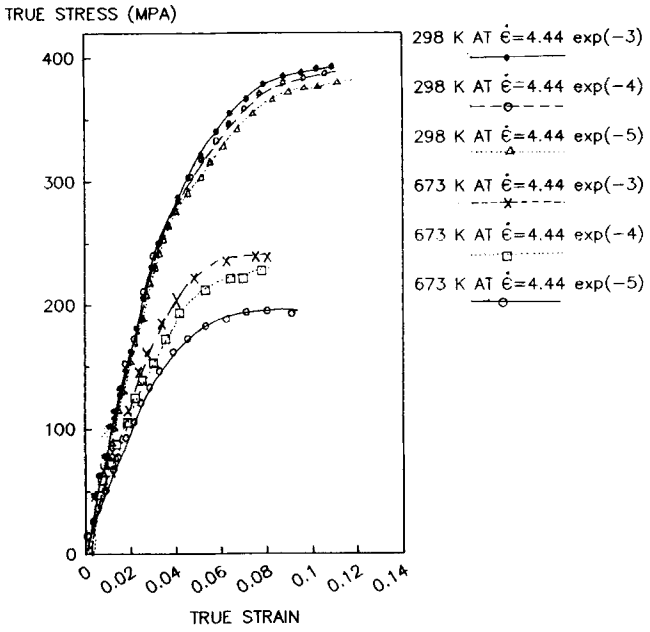

Fig. 9 True stress/true strain curve at different temperatures and strain rates

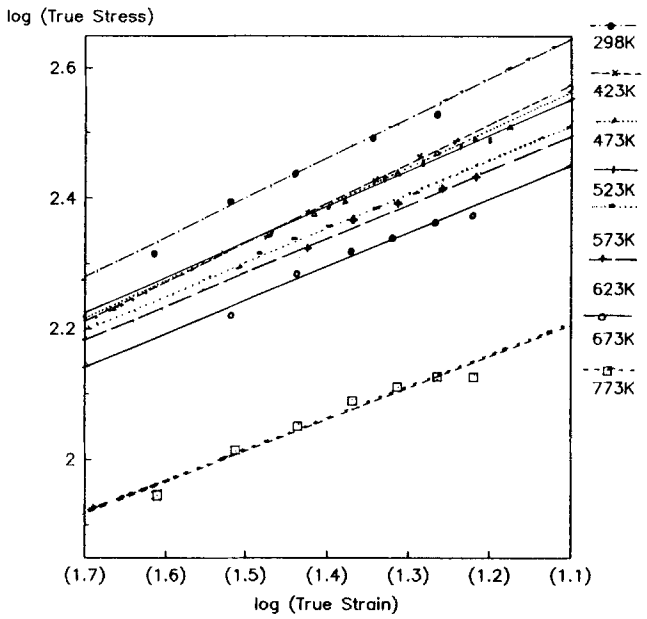

Fig. 10 Log-log curve of true stress and true strain at different temperatures and a strain rate of 4.44×10^{-4}/s

Table 2 Activation energy (Q) of the self-diffusion of zirconium in α-phase zirconium

Q, kJ/mol	Ref
92.8	11
92.8	12
92.8	13
113.9	14
Present work	
86.6	Fig. 6
99.8	Fig. 7

shown in Fig. 12. These m values were then plotted against temperature (Fig. 13) and the following observations made:

- Strain-rate sensitivity, m, increases with temperature continuously.
- The rate of increase of m is higher from 673 K onward.

3.2 *Electron Microscopy*

The thin foils extracted from the gage sections of the samples tested at ambient temperature and at 773 K were examined by TEM. Energy-dispersive x-ray analysis (EDAX) was done to determine the constituents of the observed phases. The ambient-temperature (295 K) and high-temperature (773 K) structures are shown in Fig. 14.

The microstructure of the foil from the test coupon tested at room temperature (Fig. 14a) reveals strands of grains oriented in the longitudinal (tube axial) direction. The two-phase structure consists of elongated α-Zr grains with high dislocation density inside the grains. These α grains are surrounded by a network of grain-boundary β-Zr. The pattern and shape of α-Zr grains resemble that of a bamboo tree.

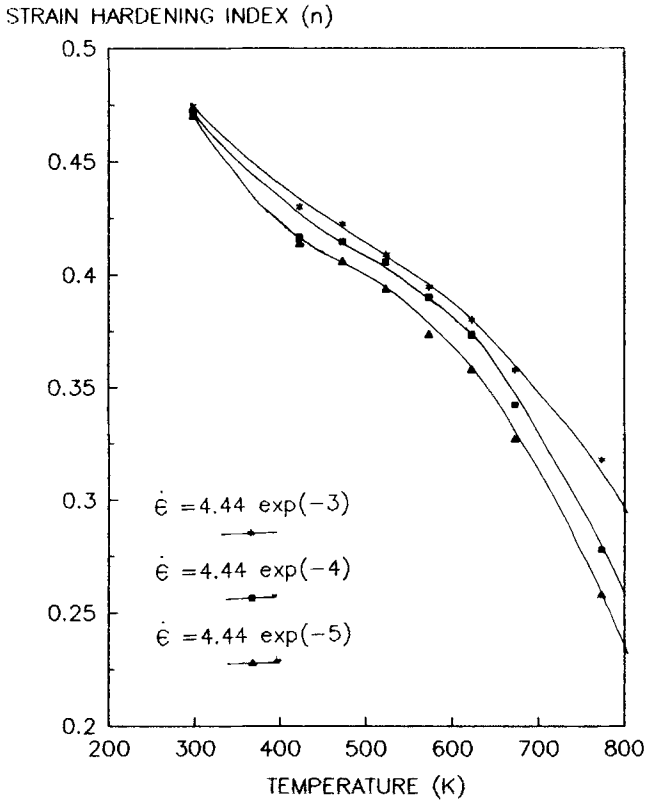

Fig. 11 Strain-hardening index as a function of test temperature at different strain rates

Figure 14(b) is from the sample tested at 773 K. The original bamboo-tree shape of the α-Zr grains has now tended to change to an equiaxed shape. The partial decomposition of the β-phase

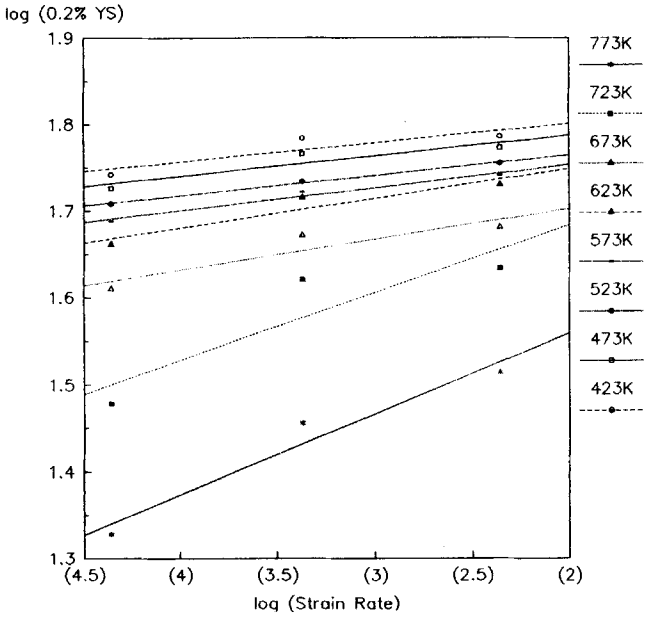

Fig. 12 Log-log plot of yield strength as a function of strain rate at different test temperatures

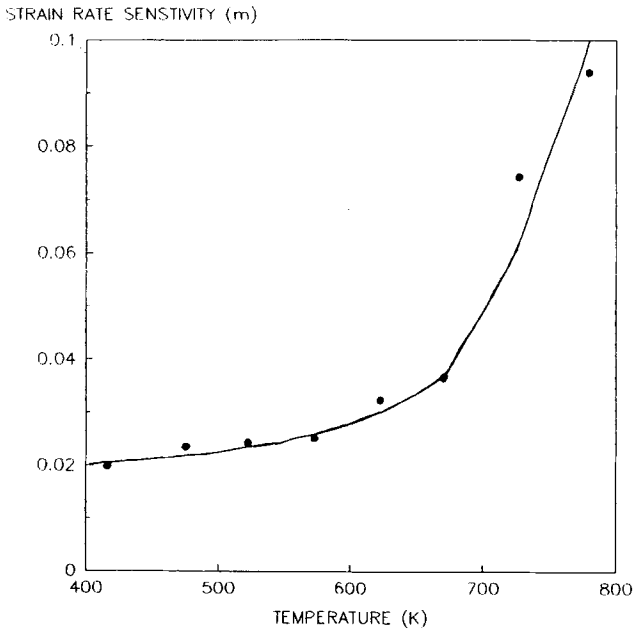

Fig. 13 Plot of strain-rate sensitivity (m) as a function of test temperature, showing that m increases rapidly beyond 673 K

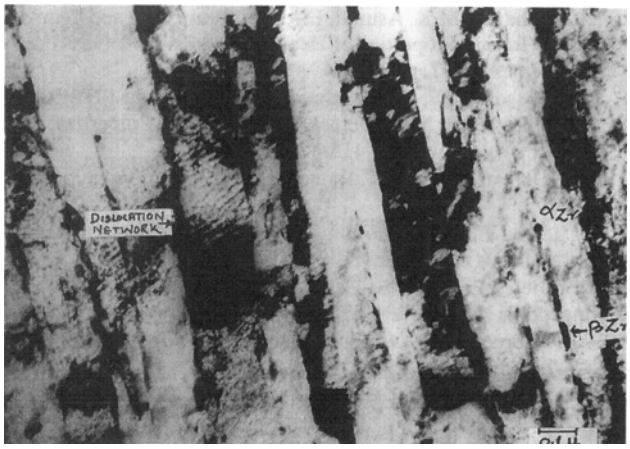

(a)

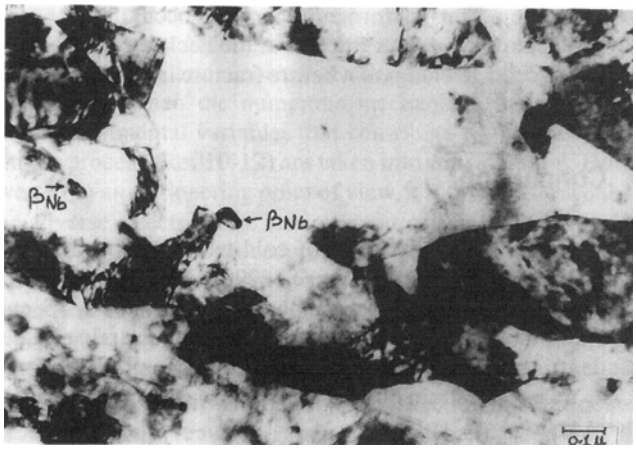

(b)

Fig. 14 TEM micrographs of Zr-2.5Nb samples taken from the gage portion of a tensile test coupon. (a) Tested at room temperature, showing bamboo-tree structure with α-Zr phase, β-Zr boundary film, and dislocation network. (b) Tested at 773 K, showing equiaxed grains with β-Nb as one of the decomposition products of β-Zr

to a fine spheroidized shape at grain boundaries is also evident. Most of the dislocation network present in Fig. 14(a) has been annihilated. This annihilation is responsible for the strain-hardening index drop at elevated temperatures.

4. Discussion

The appearance of plateaus (Fig. 2 and 3) in the material under study is a manifestation of dynamic strain aging (Ref 8-10). The activation energies of 86.6 and 99.8 kJ/mol (obtained from Fig. 6 and 7, respectively) compare favorably with the activation energy of the self-diffusion of zirconium in α-phase (Table 2).

The observed variation of strain-hardening index with temperature and strain rate can be explained on the basis of microstructure at test temperature. Strain hardening occurs as a result of interactions among dislocations during deformation. The TEM studies reveal a reduction of the dislocation network at higher temperatures. Due to this annihilation of dislocation network, strain hardening (and thus n) is lower at high temperatures. To explain the strain-rate effect on n, consider Eq 5. It is known that the strain rate imposed on the material is related to dislocation motion by:

$$\dot{\varepsilon} = \mathbf{b}\rho\bar{v} \qquad \text{(Eq 5)}$$

where ρ is the density of mobile dislocation, $\bar{v}$ is the average dislocation velocity, and **b** is an appropriate Burgers vector. The term $\bar{v}$ itself is a strong function of the shear stress (τ) required for the movement of dislocations, given by:

$$\bar{v} = (\tau/\tau_0)^{m'} \quad \text{(Eq 6)}$$

where τ_0 is resolved shear stress corresponding to unit velocity, and m' is a constant varying from 1.5 to 40 for different materials. From Eq 5 and 6, at low ρ (i.e., at higher temperature) a higher strain rate will require $\bar{v}$ to be high; hence, higher stress would be required for deformation. Thus, n is higher for higher strain rates, especially at higher temperatures.

The variation of strain-rate sensitivity of this material with temperature follows a trend similar to that of percentage elongation to fracture. The increase of percentage elongation with temperature can be attributed to two factors: the annihilation of the dislocation network present at room temperature and the formation of strain-free equiaxed grains from the elongated α-phase. The increase in strain-rate sensitivity is followed by an increase in percentage elongation to fracture. As necking begins, the strain in the necked region is higher than that in the balance gage portion. If strain-rate sensitivity is high (i.e., at high temperature), however, an increase in strain rate in the necked region leads to an increase in resistance to flow in the necked region. Thus, deformation tends to occur above or below the neck. This delays fracture at the necked region, and a higher percentage elongation before fracture is observed.

5. Conclusion

The deformation behavior of cold-worked stress-relieved Zr-2.5Nb in the temperature range of 295 to 773 K led to a number of conclusions. At higher temperatures, UTS, 0.2% YS, and the strain-hardening index (n) were found to be strain rate dependent. An approximate (quasi) plateau occurs for UTS and 0.2% YS at each strain rate. This is a manifestation of dynamic strain aging.

An empirical relationship between strength and test temperature at different strain rates was obtained. From this, the activation energy of the self-diffusion of zirconium in α-Zr was calculated.

The strain-hardening index decreased gradually from room temperature to 773 K. The value of n was higher at higher strain rates, especially at higher test temperatures. This was possibly a result of the annihilation of the dislocation network at higher temperatures.

Strain-rate sensitivity over the temperature range of 295 to 773 K followed the same trend as percentage elongation. Beyond 673 K, a sharp increase in these parameters was observed. At temperatures on the order of 773 K, most of the dislocation network present at room temperature was removed, and strain-free equiaxed grains were formed.

Acknowledgments

The authors gratefully acknowledge the support of Mr. J. Shankar Kumar (senior manager) and Mr. N. Saratchandran (director) of India's Nuclear Fuel Complex. Thanks are also due to Mr. K.K. Sinha (chief executive) and Mr. K. Balaramamoorty (former chief executive) of NFC for their continued encouragement and kind permission to publish this work. The authors also wish to thank the testing group staff for their cooperation.

References

1. R.A. Herring and D.O. Northwood, Irradiation Growth of Zirconium Alloy Pressure Tube Materials, *Mater. Nucl. Energy*, 1983, p 96-105
2. D.O. Northwood and W.L. Flong, Modifications of the Structure of Cold Worked Zr-2.5% Nb Nuclear Reactor Pressure Tube Material, *Metallography*, Vol 13, 1980, p 97-115
3. T.K. Sinha and M.K. Asundi, Effect of Strain Rate and Temperature on Tensile Properties of Heat Treated Zr-2.5% Nb Alloy, *J. Nucl. Mater.*, 1977, p 311-314
4. B.A. Cheadle, C.E. Coleman, and H. Light, Candu-PHWR Pressure Tubes: Their Manufacture, Inspection and Properties, *Nucl. Technol.*, Vol 57, 1982, p 413-429
5. A.M. Hamamad and K.K. Ramadan, *Z. Metallk.*, Vol 80, 1989, p 178
6. P. Ludwik, *Elemente der Technologischen Mechanik*, Springer, Berlin, 1960 (in German)
7. G.E. Dieter, Ed., *Mechanical Metallurgy*, 2nd ed., McGraw-Hill, Singapore, 1984, p 348-357
8. W.R. Thorpe and I.O. Smith, Tensile Properties of Zr-1% Nb Alloy, *J. Nucl. Mater.*, Vol 78, 1978, p 49-57
9. V. Ramchandran and R.E. Reed-Hill, *Metall. Trans.*, Vol 1, 1970, p 2105
10. A.M. Garde, E. Aigeltinger, B.N. Woodruff, and R.E. Reed-Hill, *Metall. Trans. A*, Vol 6A, 1975, p 1183
11. G.B. Federov and F.I. Zhomov, *Metall. Metalloved. Chistykh Met.*, Vol 1, 1959, p 162
12. P.L. Gruzin, V.S. Yemel Yanov, G.C. Ryabova, and G.B. Federov, in *Proc. Int. Conf. Peaceful Uses of Atomic Energy*, 1958, p 187
13. Ye.V. , *Metall. Met.*, Vol 1, 1958, p 196
14. F. Dyment and C.M. Libanti, *J. Mater. Sci.*, Vol 3, 1968, p 349